An Improved Method for Reconstructing Antenna Radiation Pattern in a Loaded Reverberation Chamber

Junhao Zheng, Xiaoming Chen, *Senior Member, IEEE*, Xiaobo Liu, Ming Zhang, Binhui Liu, and Yi Huang, *Fellow, IEEE*

***Abstract*—It has been experimentally demonstrated that the antenna pattern can be reconstructed using correlation coefficients and spherical wave expansion in a well-stirred large reverberation chamber (RC) when the antenna under test (AUT) has little impact on the testing environment. But the method becomes ineffective for loaded RCs. To solve this problem, we apply a compensation method to the pattern reconstruction process by using a reference antenna, enabling AUT pattern reconstruction in a loaded RC. In the proposed method, the original radiation pattern of the reference antenna is measured in an anechoic chamber (AC), and the transmission coefficients of the reference antenna are obtained according to the spherical wave coefficient expansion theory. Then, by rotating the reference antenna in the RC, the corresponding antenna correlation and autocorrelation coefficients are obtained, and the radiation pattern of the AUT is reconstructed by using the least square method. Finally, the near-field spherical scattering signals of the reference antenna are used to compensate for the reconstructed results of the AUT spherical wave coefficients, and an improved far-field radiation pattern of the AUT is obtained. The feasibility and effectiveness of the proposed method are verified by simulation and measurement in a loaded RC.**

***Index Terms*—Antenna measurement, radiation pattern reconstruction, correlation coefficient, spherical wave coefficient, least square method.**

I. Introduction

Reverberation chamber (RC) and anechoic chamber (AC) are two popular testing environments that have been widely used in various antenna measurements. The antenna radiation pattern can be readily measured in an AC. To reduce the AC space and to increase the testing speed, multi-probe AC for spherical near-field measurement is introduced (cf. Fig. 1). The far-field radiation pattern of the antenna under test (AUT) can be obtained by near-field to far-field transformation [1], [2]. Compared with ACs, the RC (cf. Fig. 2) has significant advantages in terms of cost and testing volume [3]. Therefore, it finds applications in various over-the-air (OTA) tests of antenna systems [4]-[10]. Recently, the RC-based OTA tests become even more popular thanks to the success of Internet-of-things (IoT), because the IoT requires inexpensive OTA testing solutions. The RC is usually used for measuring non-directional metrics such as antenna efficiency [9], total radiated power (TRP) and total isotropic sensitivity (TIS) of a wireless device [10]. Nevertheless, with the help of sophisticated data processing algorithms, antenna patterns can be measured in the RCs as well (at the cost of increased time) [11]-[16]. This research topic attracts lots of attentions in both academia and industry because it is highly desirable to be able to measure the antenna pattern of an IoT device in the same testing environment as for its TRP and TIS tests. For this application though, it usually suffices to have a rough estimation of the radiation pattern (with a decent main lobe estimate) of the inexpensive IoT device [17].

Currently, the methods of measuring antenna radiation patterns in RCs include the K-factor-based method [11]-[13], Doppler frequency-based method [14], [15] and correlation coefficient-based reconstruction method [16]. The correlation coefficient reconstruction method uses the RC to measure the correlation coefficients of the AUT at different orientations and reconstructs the three-dimensional radiation pattern of the AUT through the least square method. Thus, it does not require wideband AUT or time-consuming measurement as opposed to other RC-based pattern retrieval methods. And it has been experimentally verified. Nevertheless, the method assumes that the AUT has little impact on the testing environment during measurement rotation and that the field in the RC follows the isotropic distribution. This dictates a well-stirred large RC. In order to tune the frequency selectivity (coherence bandwidth) of the testing channel for OTA applications, the RC is usually loaded with lossy objects [8], which inevitably causes anisotropy of the field in the RC [18]. Sometimes, a certain amount of loading is fixed (or glued) on the sidewall of the RC (to guarantee a minimum amount of mode density for OTA tests) in a way that it is inconvenient to remove them. Unfortunately, the correlation coefficient reconstruction method [16] (referred to as a conventional method in this work) does not work properly in a loaded RC. In this work, we try to tackle this challenging problem, i.e., to reconstruct the AUT

This work was supported in part by the National Natural Science Foundation of China under Grant 62171362. (*Corresponding author: Xiaoming Chen*)

J. Zheng, X. Chen, X. Liu, M. Zhang is with the School of Information and Communication Engineering, Xi'an Jiaotong University, Xi'an 710049, China (e-mail: xiaoming.chen@mail.xjtu.edu.cn).

B. Liu is with the 5th Electronic Research Institute, Ministry of Industry and Information Technology, Guangzhou 511370, China.

Y. Huang is with the Department of Electrical Engineering and Electronics, University of Liverpool, Liverpool L69 3GJ, UK.

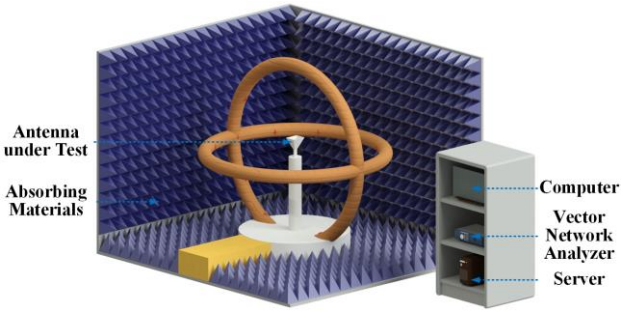

Fig. 1. Antenna measurement in an AC environment.

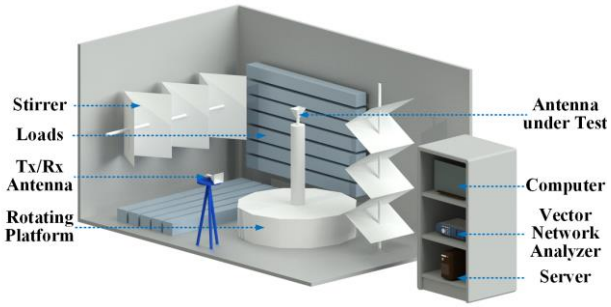

Fig. 2. Antenna measurement in an RC environment.

pattern in a loaded RC.

This paper proposes an improved method of pattern reconstruction in a loaded RC. To that end, a reference antenna with known radiation characteristics is used to probe the small loaded RC. Since the AUT and the reference antenna are measured in the same RC environment, the samples gathered by the reference antenna can be utilized to partially compensate for the non-ideal effects of the loaded RC. The detailed method and measurement procedures will be given in the next section.

II. THEORY

In order to reconstruct the AUT pattern in the RC, the relationship between correlation coefficients and radiation pattern should be firstly expressed from a forward point of view, and then the reconstruction method can be derived in a reverse method. For the sake of completeness, this section first presents the spherical wave expansion theory and the correlation coefficient reconstruction algorithm before introducing the proposed method.

According to the theory of spherical wave expansion, the far-field of the AUT can be expanded into a summation of spherical wave modes. Denoting the minimum spherical radius of the antenna as r_0, the electric field outside the minimum sphere ($r > r_0$) can be expressed as [1]

$$\boldsymbol{E}(r,\theta,\phi)=\sum_{n=1}^{N}\sum_{m=-n}^{n}\left\{a_{mn}\boldsymbol{M}_{mn}(r,\theta,\phi)+b_{mn}\boldsymbol{N}_{mn}(r,\theta,\phi)\right\} \quad (1)$$

where a_{mn} and b_{mn} represent the complex spherical wave coefficients, $\boldsymbol{M}_{mn}(r,\theta,\varphi)$ and $\boldsymbol{N}_{mn}(r,\theta,\varphi)$ represent the spherical wave generating functions, and $N=[kr_0+10]$ (i.e., the smallest integer that is larger than kr_0+10 with k being the free-space wavenumber) represents the order of the spherical expansion mode.

From the spherical near-field expansion in Eq. (1), it can be seen that the far-field components of the AUT can be represented by the spherical wave coefficients. Besides, the correlation coefficients between different antennas are determined from the antenna radiation patterns. Therefore, the antenna correlation coefficients can be readily calculated by utilizing the orthogonality between the spherical wave modes.

Given an AUT, we choose a proper reference antenna whose radiation pattern is measured in an AC beforehand. The radiation patterns of the reference antenna and AUT are denoted as $\boldsymbol{E}_1(\theta,\varphi)$ and $\boldsymbol{E}_2(\theta,\varphi)$, respectively. The correlation between the two antennas can be calculated as follows [19], [21]

$$\rho_0=\frac{\left|\iint \boldsymbol{E}_1(\theta,\varphi)\bullet\boldsymbol{E}_2^*(\theta,\varphi)d\Omega\right|}{\sqrt{\iint\left|\boldsymbol{E}_1(\theta,\varphi)\right|^2 d\Omega\iint\left|\boldsymbol{E}_2(\theta,\varphi)\right|^2 d\Omega}} \quad (2)$$

where $d\Omega=\sin\theta d\theta d\varphi$. According to the near-field to far-field transformation theory [1], [22], the generating functions $\boldsymbol{M}_{mn}(r,\theta,\varphi)$ and $\boldsymbol{N}_{mn}(r,\theta,\varphi)$ in Eq. (1) satisfy the following orthogonality relations

$$\begin{aligned}
&\iint \boldsymbol{M}_{mn}\bullet\boldsymbol{M}^*_{m'n'}\sin\theta d\theta d\varphi=\begin{cases}0,(m,n)\neq(m',n')\\1,(m,n)=(m',n')\end{cases}\\
&\iint \boldsymbol{N}_{mn}\bullet\boldsymbol{N}^*_{m'n'}\sin\theta d\theta d\varphi=\begin{cases}0,(m,n)\neq(m',n')\\1,(m,n)=(m',n')\end{cases}\\
&\iint \boldsymbol{N}_{mn}\bullet\boldsymbol{M}^*_{m'n'}\sin\theta d\theta d\varphi=0
\end{aligned} \quad (3)$$

where vectors $\boldsymbol{M}^*_{m'n'}$ and $\boldsymbol{N}^*_{m'n'}$ represent the adjoint spherical wave generating functions under different expansion orders. Through the orthogonality principle of Eq. (3), Eq. (2) can be rewritten as

$$\rho_0=\frac{\left|\sum_{n=1}^{N}\sum_{m=-n}^{n}\left(a_{mn1}a^*_{mn2}+b_{mn1}b^*_{mn2}\right)\right|}{\sqrt{\sum_{n=1}^{N}\sum_{m=-n}^{n}\left\|a_{mn1}+b_{mn1}\right\|^2\sum_{n=1}^{N}\sum_{m=-n}^{n}\left\|a_{mn2}+b_{mn2}\right\|^2}} \quad (4)$$

where (a_{mn1},b_{mn1}) and (a_{mn2},b_{mn2}) represent the spherical wave coefficients of $\boldsymbol{E}_1(\theta,\varphi)$ and $\boldsymbol{E}_2(\theta,\varphi)$, respectively. Now, it is clear that the forward process of deriving the correlation coefficients ρ_0 is determined by the spherical wave coefficients. Accordingly, the reverse problem of reconstructing the radiation pattern of the AUT can be calculated by the correlation coefficient matrix.

The reconstruction problem is to obtain the unknown AUT spherical wave coefficients (a_{mn2},b_{mn2}) through multiple groups of known spherical wave coefficients (a_{mn1},b_{mn1}) of the reference antenna and the correlation coefficients vector $\boldsymbol{\rho}_{Corr}=(\rho_{0,\alpha},\rho_{0,\beta},\rho_{0,\gamma})^T$ in different rotation angles, where α, β and γ mean that the antenna is rotated around the x axis with angle α, then rotated around y axis with angle β, and

finally rotated around z axis with angle γ.

Then the reconstruction expression can be written as

$$\boldsymbol{M}_{AUT} = \boldsymbol{M}_{REF}^{+}\boldsymbol{\rho}_{Corr} \tag{5}$$

where $\boldsymbol{M}_{AUT} = (a_{-1,1,2} \cdots a_{N,N,2}\ b_{-1,1,2} \cdots b_{N,N,2})^{H}$ represents the AUT spherical wave coefficient vector, and $\boldsymbol{M}_{REF}^{+}$ is the Moore-Penrose pseudoinverse matrix of the spherical wave coefficients under different rotation angles for the reference antenna, which can be expressed as

$$\boldsymbol{M}_{REF}^{+} = \begin{bmatrix} a_{-1,1,1,\alpha_1} & \cdots & a_{N,N,1,\alpha_1} & b_{-1,1,1,\alpha_1} & \cdots & b_{N,N,1,\alpha_1} \\ \vdots & \ddots & \vdots & \vdots & \ddots & \vdots \\ a_{-1,1,1,\alpha_{NUM}} & \cdots & a_{N,N,1,\alpha_{NUM}} & b_{-1,1,1,\alpha_{NUM}} & \cdots & b_{N,N,1,\alpha_{NUM}} \\ a_{-1,1,1,\beta_1} & \cdots & a_{N,N,1,\beta_1} & b_{-1,1,1,\beta_1} & \cdots & b_{N,N,1,\beta_1} \\ \vdots & \ddots & \vdots & \vdots & \ddots & \vdots \\ a_{-1,1,1,\beta_{NUM}} & \cdots & a_{N,N,1,\beta_{NUM}} & b_{-1,1,1,\beta_{NUM}} & \cdots & b_{N,N,1,\beta_{NUM}} \\ a_{-1,1,1,\gamma_1} & \cdots & a_{N,N,1,\gamma_1} & b_{-1,1,1,\gamma_1} & \cdots & b_{N,N,1,\gamma_1} \\ \vdots & \ddots & \vdots & \vdots & \ddots & \vdots \\ a_{-1,1,1,\gamma_{NUM}} & \cdots & a_{N,N,1,\gamma_{NUM}} & b_{-1,1,1,\gamma_{NUM}} & \cdots & b_{N,N,1,\gamma_{NUM}} \end{bmatrix}^{+} \tag{6}$$

where NUM is the total number of the rotation angles in any one of the three axes, and $\boldsymbol{M}_{REF}$ is the matrix of the (a_{mn1}, b_{mn1}) under different rotation angles $\alpha_1, \ldots, \alpha_{NUM}$, $\beta_1, \ldots, \beta_{NUM}$, $\gamma_1, \ldots, \gamma_{NUM}$, where each row represents all the coefficients (a_{mn1}, b_{mn1}) with the expansion mode ranging from 1 to N under a fixed rotation angle. Since the matrix $\boldsymbol{M}_{REF}^{+}$ can be formed by the radiation pattern of the reference antenna under different rotation angles, then Eq. (4) can be rewritten as

$$\rho_0 = \frac{\left|\sum_{n=1}^{N}\sum_{m=-n}^{n}((R_{mna}a_{mn1})a_{mn2}^{*} + (R_{mnb}b_{mn1})b_{mn2}^{*})\right|}{\sqrt{\sum_{n=1}^{N}\sum_{m=-n}^{n}\left\|R_{mna}a_{mn1} + R_{mnb}b_{mn1}\right\|^2 \sum_{n=1}^{N}\sum_{m=-n}^{n}\left\|a_{mn2} + b_{mn2}\right\|^2}} \tag{7}$$

where R_{mna} and R_{mnb} are the rotation coefficients for a_{mn1} and b_{mn1}. In addition, the correlation coefficients ρ_0 can also be obtained by measuring the S-parameters in the RC [19], [20]

$$\rho_0 = \frac{\left|\sum_{k=1}^{K}(S_{21,k,REF} - \langle S_{21,REF}\rangle)(S_{21,k,AUT} - \langle S_{21,AUT}\rangle)^{*}\right|}{\sqrt{\sum_{k=1}^{K}\left|S_{21,k,REF} - \langle S_{21,REF}\rangle\right|^2 \sum_{k=1}^{K}\left|S_{21,k,AUT} - \langle S_{21,AUT}\rangle\right|^2}} \tag{8}$$

where $S_{21,k,REF}$ and $S_{21,k,AUT}$ are the measured S-parameters from Tx antenna to the reference antenna and the AUT, respectively. $\langle S_{21,REF}\rangle$ and $\langle S_{21,AUT}\rangle$ are the average S-parameters of the $K = N_{Freq} \times N_{Mech}$ samples, where N_{Freq} and N_{Mech} are the number of frequency stirring and mechanical stirring, respectively. If N_{Freq} and N_{Mech} are large enough, then $\langle S_{21,REF}\rangle$ and $\langle S_{21,AUT}\rangle$ approaches to zero.

Since the radiated powers of the AUT and reference antenna are the same (assuming negligible losses in the antennas), the reconstruction expressions can be derived from (7) and (8) as

$$\begin{cases} \dfrac{\left|\sum_{n=1}^{N}\sum_{m=-n}^{n}((R_{mna,\alpha}a_{mn1})a_{mn2}^{*} + (R_{mnb,\alpha}b_{mn1})b_{mn2}^{*})\right|}{\sum_{n=1}^{N}\sum_{m=-n}^{n}\left\|a_{mn1} + b_{mn1}\right\|^2} = \rho_{0,\alpha} \\ \dfrac{\left|\sum_{n=1}^{N}\sum_{m=-n}^{n}((R_{mna,\beta}a_{mn1})a_{mn2}^{*} + (R_{mnb,\beta}b_{mn1})b_{mn2}^{*})\right|}{\sum_{n=1}^{N}\sum_{m=-n}^{n}\left\|a_{mn1} + b_{mn1}\right\|^2} = \rho_{0,\beta} \\ \dfrac{\left|\sum_{n=1}^{N}\sum_{m=-n}^{n}((R_{mna,\gamma}a_{mn1})a_{mn2}^{*} + (R_{mnb,\gamma}b_{mn1})b_{mn2}^{*})\right|}{\sum_{n=1}^{N}\sum_{m=-n}^{n}\left\|a_{mn1} + b_{mn1}\right\|^2} = \rho_{0,\gamma} \end{cases} \tag{9}$$

where $R_{mna,\alpha}$, $R_{mnb,\alpha}$, $R_{mna,\beta}$, $R_{mnb,\beta}$, $R_{mna,\gamma}$, and $R_{mnb,\gamma}$ are the projection of rotation coefficients R_{mna} and R_{mnb} in the x, y, and z axes with rotation angles of α, β, and γ, respectively, and $\rho_{0,\alpha}$, $\rho_{0,\beta}$, and $\rho_{0,\gamma}$ are the calculated correlation coefficients using the measured S-parameters in Eq. (8) along the three axes. Then, combining Eqs. (5)-(9), the spherical wave coefficient matrix $\boldsymbol{M}_{AUT}$ of the AUT can be derived.

The above method approximately holds for a large well-stirred RC without absorbing loads. When the RC loading causes anisotropy, the conventional reconstruction algorithm produces poor results. In this case, a compensation method can be used to improve the pattern reconstruction accuracy, as will be shown later.

Since the RC environment keeps the same when the reference antenna and the AUT are under test, the excitation signals derived by the spherical wave coefficients of the two antennas are in good consistency. According to the antenna transmission coefficients [23]-[27] and the mode expansion theory [28], [29], and ignoring parameters which are irrelevant to θ and φ, the far-field pattern can be expressed as

$$\begin{aligned} \boldsymbol{E}(\theta,\phi) &= \frac{k}{\sqrt{\eta}}\sum_{n=1}^{N}\sum_{m=-n}^{n} T_{smn}v\boldsymbol{F}_{smn}^{3}(\theta,\phi) \\ &= \frac{k}{\sqrt{\eta}}\sum_{n=1}^{N}\sum_{m=-n}^{n}\left\{T_{1mn}v\boldsymbol{F}_{1mn}^{3}(\theta,\phi) + T_{2mn}v\boldsymbol{F}_{2mn}^{3}(\theta,\phi)\right\} \end{aligned} \tag{10}$$

where v and T_{smn} represent the excitation signals and transmission coefficients of the antenna, respectively. F_{smn}^{3} is the outgoing spherical wave generating functions [29].

From Eqs. (1) and (10), it can be known that $T_{1mn}v = a_{mn}$ and $T_{2mn}v = b_{mn}$. Thus, the relationship between the transmission coefficients and the spherical wave coefficients can be given as

$$T_{smn}v = (a_{mn}, b_{mn}) \tag{11}$$

The transmission coefficients $T_{smn,REF}$ of the reference antenna can be calculated by [1]. Thus, when $T_{smn,REF}$ is

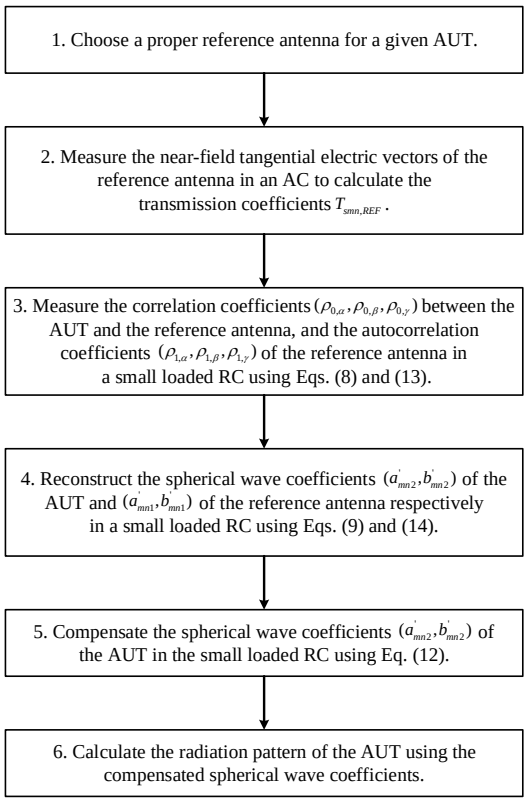

Fig. 3. Flowchart of the proposed method.

obtained, the proposed method can be realized as follows.

Applying the relationship of Eq. (11) to the RC correlation coefficient reconstruction described in Eqs. (1)-(9), it can be found that the ideal (a_{mn},b_{mn}) obtained in a well-stirred RC and the non-ideal (a'_{mn},b'_{mn}) obtained in a loaded RC all satisfy the relationship of Eq. (11). Besides, the antenna transmission coefficients T_{smn} keep unchanged in any conditions, and the excitation signals v also remain stable for the same RC environment. Then the following relationship can be obtained

$$\boldsymbol{T}_{s,AUT}=(\boldsymbol{B}'_{s,2})((\boldsymbol{T}_{s,REF})^{+}(\boldsymbol{B}'_{s,1}))^{+} \tag{12}$$

where $\boldsymbol{T}_{s,AUT}$ and $\boldsymbol{T}_{s,REF}$ are the $(2N+1)$-by-N transmission coefficient matrices of the AUT and reference antenna, respectively, $\boldsymbol{B}'_{s,2}$ and $\boldsymbol{B}'_{s,1}$ are the $(2N+1)$-by-N spherical wave coefficient matrices measured in the loaded RC for the AUT and reference antenna, respectively. When the index $s=1$, Eq. (12) can get the transmission coefficients $T_{1mn,AUT}$ of the spherical wave coefficients a'_{mn2} for the AUT; when $s=2$, Eq. (12) can be used to derive $T_{2mn,AUT}$ of b'_{mn2} for the AUT.

Therefore, when $T_{smn,REF}$ is determined in an AC beforehand, and (a'_{mn2},b'_{mn2}) and (a'_{mn1},b'_{mn1}) are measured in the loaded RC, then $T_{smn,AUT}$ of the AUT can be drawn. Finally, the compensated pattern reconstruction of the AUT can be obtained in the loaded RC.

It should be noted that Eqs. (2)-(9) are the expressions of the correlation coefficients between the AUT and reference antenna, which can be used to derive (a'_{mn2},b'_{mn2}) and the non-ideal AUT pattern. Thus, in order to calculate the non-ideal reconstruction pattern and (a'_{mn1},b'_{mn1}) of the reference antenna in the loaded RC, the autocorrelation coefficients $\boldsymbol{\rho}_{Auto}=(\rho_{1,\alpha},\rho_{1,\beta},\rho_{1,\gamma})^{T}$ should be determined.

In Eq. (8), $S_{21,k,REF}$ and $\langle S_{21,REF}\rangle$ are measured by rotating the reference antenna along the x, y and z axes, while $S_{21,k,AUT}$ and $\langle S_{21,AUT}\rangle$ are measured with the static AUT. Therefore, replacing $S_{21,k,AUT}$ and $\langle S_{21,AUT}\rangle$ in Eq. (8) with $S'_{21,k,REF}$ and $\langle S'_{21,REF}\rangle$ of the static reference antenna, and the autocorrelation coefficients ρ_1 can then be derived as

$$\rho_1=\frac{\left|\sum_{k=1}^{K}(S_{21,k,REF}-\langle S_{21,REF}\rangle)(S'_{21,k,REF}-\langle S'_{21,REF}\rangle)^{*}\right|}{\sqrt{\sum_{k=1}^{K}\left|S_{21,k,REF}-\langle S_{21,REF}\rangle\right|^{2}\sum_{k=1}^{K}\left|S'_{21,k,REF}-\langle S'_{21,REF}\rangle\right|^{2}}} \tag{13}$$

Since the reference antenna pattern is measured in an AC and (a_{mn1},b_{mn1}) can be determined beforehand, replace $(a^{*}_{mn2},b^{*}_{mn2})$ with $((a'_{mn1})^{*},(b'_{mn1})^{*})$ in Eq. (9) that represents the unknown adjoint spherical wave coefficients of the reference antenna to be determined. Moreover, the powers of the rotated and static reference antenna are equivalent. Consequently, the reverse reconstruction method of (a'_{mn1},b'_{mn1}) of the reference antenna can be expressed as

$$\begin{cases}\dfrac{\left|\sum_{n=1}^{N}\sum_{m=-n}^{n}((R_{mna,\alpha}a_{mn1})(a'_{mn1})^{*}+(R_{mnb,\alpha}b_{mn1})(b'_{mn1})^{*})\right|}{\sum_{n=1}^{N}\sum_{m=-n}^{n}\|a_{mn1}+b_{mn1}\|^{2}}=\rho_{1,\alpha}\\ \dfrac{\left|\sum_{n=1}^{N}\sum_{m=-n}^{n}((R_{mna,\beta}a_{mn1})(a'_{mn1})^{*}+(R_{mnb,\beta}b_{mn1})(b'_{mn1})^{*})\right|}{\sum_{n=1}^{N}\sum_{m=-n}^{n}\|a_{mn1}+b_{mn1}\|^{2}}=\rho_{1,\beta}\\ \dfrac{\left|\sum_{n=1}^{N}\sum_{m=-n}^{n}((R_{mna,\gamma}a_{mn1})(a'_{mn1})^{*}+(R_{mnb,\gamma}b_{mn1})(b'_{mn1})^{*})\right|}{\sum_{n=1}^{N}\sum_{m=-n}^{n}\|a_{mn1}+b_{mn1}\|^{2}}=\rho_{1,\gamma}\end{cases} \tag{14}$$

As can be seen, the proposed reconstruction method needs to know the transmission coefficients $T_{smn,REF}$, the correlation coefficients $(\rho_{0,\alpha},\rho_{0,\beta},\rho_{0,\gamma})$ between the AUT and reference antenna, the autocorrelation coefficients $(\rho_{1,\alpha},\rho_{1,\beta},\rho_{1,\gamma})$ of the reference antenna, and the non-ideal spherical wave coefficients (a'_{mn1},b'_{mn1}) and (a'_{mn2},b'_{mn2}). Through the process above, the AUT radiation pattern can be reconstructed and compensated by the reference antenna in a loaded RC.

Fig. 3 shows a flowchart of the proposed method for better illustration.

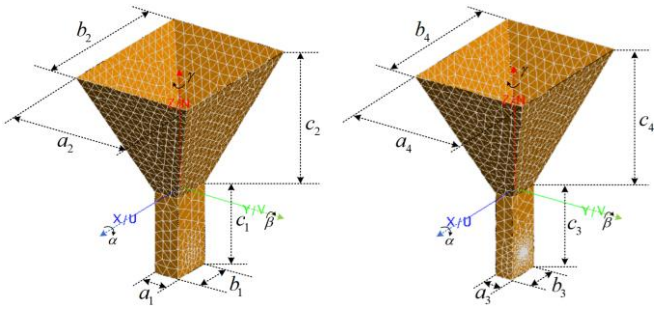

(a) (b)

Fig. 4. Configuration of the AUT and reference antenna. (a) AUT; (b) reference antenna.

TABLE I
ANTENNA MODELING PARAMETERS

Waveguide size/cm		Horn size/cm	
a_1	9.48	a_2	45.80
b_1	15.96	b_2	58.00
c_1	30.20	c_2	46.00
a_3	6.48	a_4	42.80
b_3	12.96	b_4	55.00
c_3	30.20	c_4	46.00

Step 1: In order to reconstruct the AUT radiation pattern, the reference antenna must be larger than the AUT. According to [1], [28] and [29], it can be found that the expansion order is $N=[kr_0]+10$, the diameter of the minimum sphere is $D=2r_0$ ($r_0 \cong N/k$), and the Rayleigh distance is $R=2D^2/\lambda$. Thus a large reference antenna will increase D, r_0 and N, and is more sensitive to a large number of modes, resulting in a better characterization of the test zone field (TZF) and more accurate pattern reconstruction.

Step 2: Since the compensation method in Eq. (12) relies on the spherical wave coefficients and the excitation signals v, which are theoretically consistent for the two antennas in the RC environment, the radiation pattern of the reference antenna should be measured in an AC beforehand to obtain the transmission coefficients $T_{smn,REF}$, [1] and [29].

Step 3: In a loaded RC, the non-ideal correlation coefficients $(\rho_{0,\alpha},\rho_{0,\beta},\rho_{0,\gamma})$ and the autocorrelation coefficients $(\rho_{1,\alpha},\rho_{1,\beta},\rho_{1,\gamma})$ are measured using Eqs. (8) and (13).

Step 4: Then, the Moore-Penrose pseudoinverse matrix can be used with $(\rho_{0,\alpha},\rho_{0,\beta},\rho_{0,\gamma})$ and $(\rho_{1,\alpha},\rho_{1,\beta},\rho_{1,\gamma})$ to reconstruct (a'_{mn2},b'_{mn2}) and (a'_{mn1},b'_{mn1}) of the AUT and reference antenna respectively.

Step 5: When the non-ideal (a'_{mn1},b'_{mn1}) and (a'_{mn2},b'_{mn2}) are derived, the compensation method in Eq. (12) is used to alleviate the adverse effects of the loaded RC on (a'_{mn2},b'_{mn2}).

Step 6: Finally, the compensated spherical wave coefficients (a'_{mn2},b'_{mn2}) of the AUT can be obtained and the radiation pattern can then be improved.

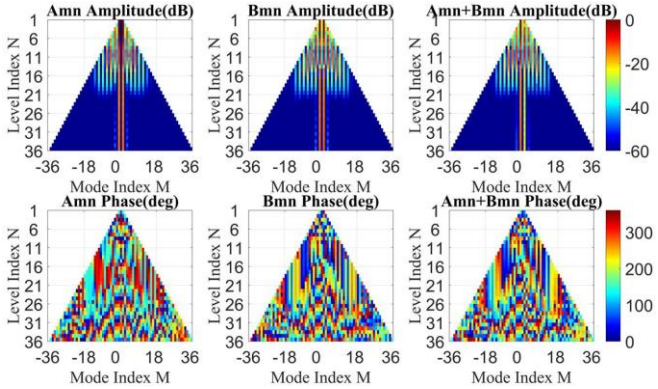

Fig. 5. Amplitude and phase of the AUT spherical wave coefficients.

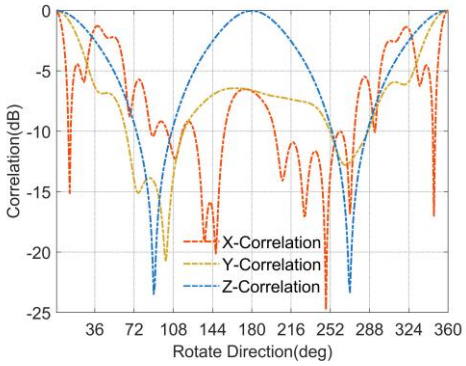

Fig. 6. Correlation coefficients between the AUT and reference antenna along the x,y,z axes under the angular restriction.

III. SIMULATIONS AND MEASUREMENTS

In this section, the simulation and measurement results are shown in order to prove the effectiveness of the proposed method.

A. Simulations

The AUT and reference antenna (cf. Fig. 4) simulation models are constructed in the FEKO software and the antenna parameters are listed in Table I.

The voltage amplitude on the waveguide port is normalized, and the working frequency is 1 GHz. The data sampling interval in θ and φ is 5° with a minimum spherical radius of 10λ. In the subsequent simulation processing, the spherical scattering signals are limited in specific angular ranges with $\varphi=(0^\circ\sim360^\circ)$ and $\theta=(40^\circ\sim108^\circ)$ to emulate the influence of absorbing loads in the RC (see [18] for example).

The AUT radiation pattern can be obtained from the full-wave simulation in FEKO, and the decomposition into (a_{mn2},b_{mn2}) are then calculated and shown in Fig. 5, where the coefficients are expanded with a mode order of 36. In Fig. 5, the amplitude and phase of (a_{mn2},b_{mn2}) are plotted as pyramids, and the absolute values of the amplitude are decreased with the increase of the mode index. Besides, it can be seen that the amplitudes of the spherical wave coefficients are more relevant when comparing differences before and after the reconstruction process; the phase plots offer limited information and, therefore

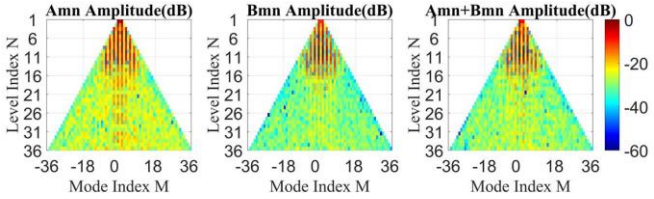

Fig. 7. Reconstructed amplitude of the AUT spherical wave coefficients under the angular restriction.

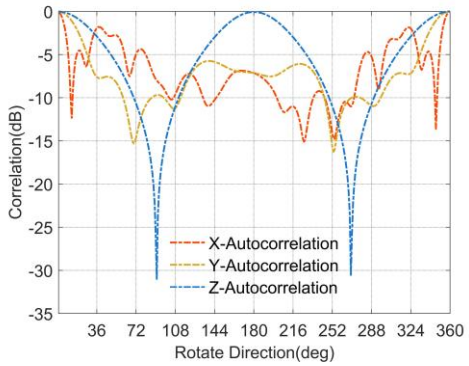

Fig. 8. Autocorrelation coefficients of the reference antenna along the x, y, z axes under the angular restriction.

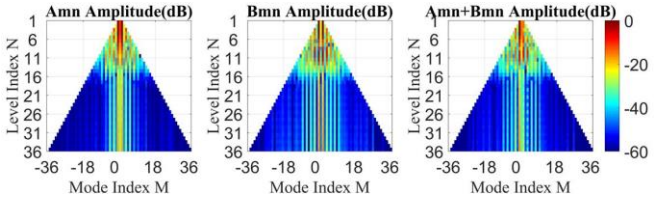

Fig. 9. Compensated amplitude of the AUT spherical wave coefficients.

, are omitted after.

Appling the angular restriction of the loaded RC to the radiation pattern of the AUT and rotating the reference antenna with an interval of 1° along x, y and z axes, the correlation coefficients $(\rho_{0,\alpha}, \rho_{0,\beta}, \rho_{0,\gamma})$ between the AUT and the rotated reference antenna can be calculated using Eq. (7) and plotted in Fig. 6. The non-ideal reconstructed spherical wave coefficients (a'_{mn2}, b'_{mn2}) of the AUT can be derived using Eq. (9), as shown in Fig. 7. It can be seen from the amplitudes of Fig. 5 and Fig. 7 that, without any compensation in a loaded RC, the conventional reconstruction method has poor performance due to the scattering angular limitation in a loaded RC.

Next, we follow steps 3 and 4 in the flowchart to calculate the autocorrelation coefficients $(\rho_{1,\alpha}, \rho_{1,\beta}, \rho_{1,\gamma})$ as shown in Fig. 8, and reversely calculate (a'_{mn1}, b'_{mn1}) of the reference antenna. Finally, we compensate the non-ideal (a'_{mn2}, b'_{mn2}) using Eq. (12) and the compensated reconstruction of the spherical wave coefficients of the AUT are plotted in Fig. 9. From the comparison of Figs. 5, 7 and 9, it can be known that the compensated spherical wave coefficients are in good consistency with the theoretical ones and there is an obvious improvement compared with the result in Fig. 7. The theoretical, non-ideal, and compensated three-dimensional (3-D) radiation

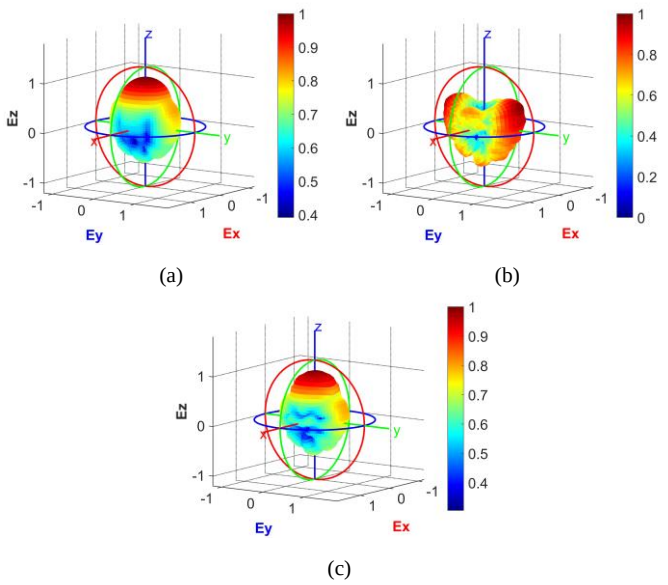

Fig. 10. Radiation pattern of the AUT: (a) theoretical pattern; (b) reconstructed pattern using the conventional method; (c) compensated pattern using the proposed method. For better illustration, the maximum value is normalized to 1 V/m.

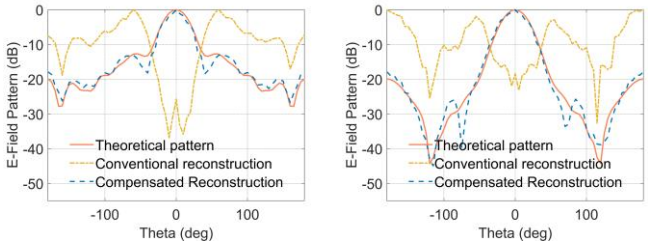

Fig. 11. Comparison of the AUT radiation pattern in (a) E-plane and (b) H-plane.

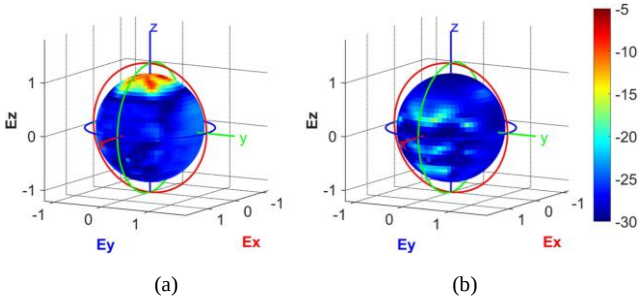

Fig. 12. Comparison of the 3-D pattern errors between the theoretical AUT pattern and (a) the non-ideal reconstructed AUT pattern; (b) the compensated reconstructed AUT pattern. The relative errors in all angles are in decibel.

patterns of the AUT are shown in Fig. 10. The theoretical gain of the simulated AUT is 13.8 dBi, while the compensated result using the proposed method is 12.5 dBi. The cutting plots in E- and H- planes are shown in Fig. 11, where the red curve represents the original theoretical pattern, the yellow curve corresponds to the non-ideal reconstructed pattern using the conventional method, and the blue curve shows the compensated results using the proposed method. From the results of the 3-D patterns and the 2-D cutting plots, it can be seen that the main lobe reconstructed by the proposed method

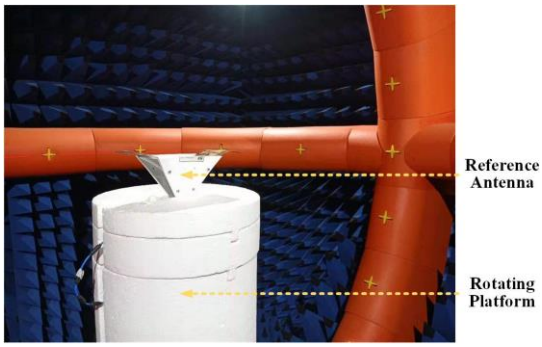

Fig. 13. Antenna radiation pattern measurement environment in a multi-probe AC.

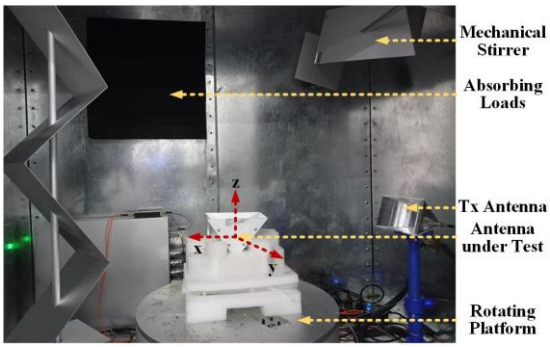

Fig. 14. Correlation coefficients measurement environment in a small loaded RC.

has a significant improvement when compared with the conventional method.

Besides, Figs. 12(a) and (b) use unit sphere to show the pattern errors between the original theoretical pattern and the two reconstructed AUT patterns obtained by the conventional and proposed method, respectively. Through the pattern errors shown in Fig. 12(a), it can be seen that the largest error between the theoretical and conventional reconstructed pattern is about -5 dB and the significant errors mainly accumulate at the top of the unit sphere. In contrast, the largest error introduced by the proposed reconstruction method is less than -15 dB (i.e., the maximum error is reduced by more than 10 dB) and a small number of errors are sparsely distributed on the unit sphere. It is clear that the proposed method outperforms the conventional one in a loaded RC. (It should be noted that the proposed method and the conventional method have similar performance in an unloaded RC. For brevity, we mainly focus on the loaded RC case in this work.)

B. Measurements

A multi-probe AC is used for the radiation pattern measurements of the reference antenna and the AUT (cf. Fig. 13). The AUT pattern measured in the AC is regarded as the true pattern for comparison with the reconstructed patterns from RC measurements, while the reference antenna pattern obtained from the AC is used for compensation of the adverse effect of the loaded RC on the reconstructed AUT pattern in a loaded RC. For experimental verifications, two RCs with different sizes are used as the testing environments. A horn antenna is used as the reference antenna, while a different horn antenna and a magneto-electric (ME) dipole antenna [30] are

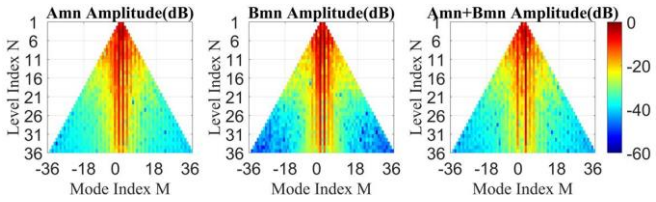

Fig. 15. Measured amplitude of the AUT spherical wave coefficients in the AC.

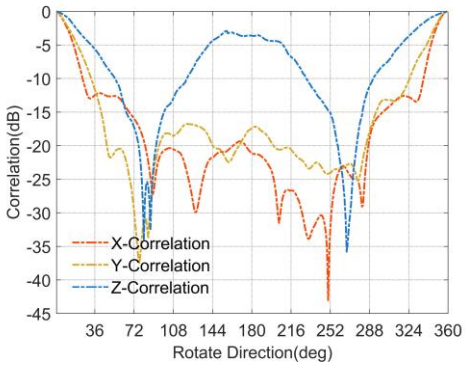

Fig. 16. Measured correlation coefficients between the AUT and the reference antenna along the x, y, z axes in the small loaded RC.

used as the AUTs.

1) Small RC and Horn AUT

Fig. 14 shows the measurement environment in a small loaded RC, where the x, y and z coordinates are marked in red lines. The RC has a size of 1.50 m × 1.44 m × 0.92 m. Besides, the absorbing loads are added on the top and side walls of the RC. Notably, the rotation of the reference antenna along the three directions is realized by sequentially making the three axes of the reference antenna perpendicular to the horizontal plane of the turntable platform. Foams are used as the support of the antenna to leave a distance of more than $\lambda/2$ at the testing frequency between the antenna and the turntable platform in order to ensure statistical uniformity in the working area of the RC [3].

The working frequency of the antennas is selected to be 2.5 GHz. The platform in RC is rotated with 1° interval. The total number of the measured samples along one axis is $N_{Sum} = N_{Mech} \times N_{Freq} \times 360$, where the number of mechanical mode stirring N_{Mech} and frequency stirring N_{Freq} are 5 and 200 with a frequency step of 1 MHz. Thus, when the platform rotates 360° around the three axes, the number of the entire samples is 1.08×10^6. Finally, after the samples are collected, $(\rho_{0,\alpha}, \rho_{0,\beta}, \rho_{0,\gamma})$ and $(\rho_{1,\alpha}, \rho_{1,\beta}, \rho_{1,\gamma})$ can be determined. Moreover, it should be noted that the turntable platform and the mode stirring are rotated separately, which means that the platform rotates 360° around the axis with the mode stirrer fixed at one position. When the turntable platform finishes one circular rotation, the mode stirrers move to the next position and keep static, and the turntable platform rotates 360° again. Accordingly, the AUT measurement time is $T_1 = N_{Direc} \times N_{Mech} \times T_{Freq} = 5\,\text{min}$, while the reference antenna

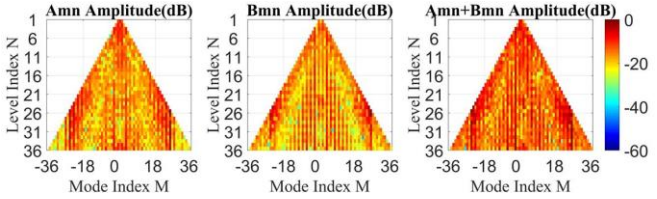

Fig. 17. Reconstructed amplitude of the AUT spherical wave coefficients in the small loaded RC.

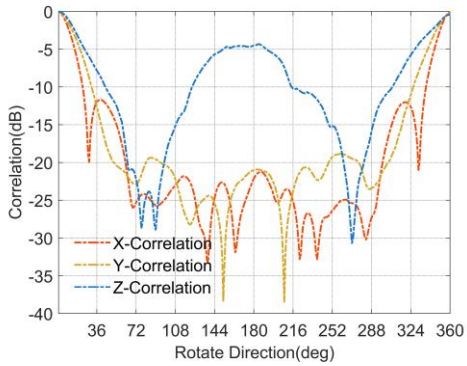

Fig. 18. Measured autocorrelation coefficients of the reference antenna along the x, y, z axes in the small loaded RC.

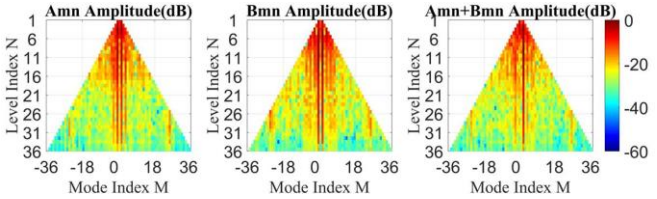

Fig. 19. Compensated amplitude of the AUT spherical wave coefficients in the small loaded RC.

testing time is $T_2 = N_{Direc} \times N_{Mech} \times 360 \times T_{Freq} = 255\,\text{min}$, where N_{Direc} represents the number of three directions in x, y, and z, and T_{Freq} represents the frequency stirring time. So, the entire test time of a single AUT is 4.3 hours ($T_1 + T_2$). Note that in practice, however, the reference measurement ($T_2 = 255$ min) can be performed beforehand, and used repeatedly for field compensation of different AUT measurements (each takes $T_1 = 5$ min). In this case, the proposed method becomes time efficient.

The "ideal" spherical wave coefficients of the AUT measured in the AC are shown in Fig. 15, and the correlation coefficients $(\rho_{0,\alpha}, \rho_{0,\beta}, \rho_{0,\gamma})$ obtained by the small loaded RC are plotted in Fig. 16. The non-ideal spherical wave coefficients obtained by using Eq. (9) are shown in Fig. 17.

Following the processes presented in the previous section, the measured autocorrelation coefficients $(\rho_{1,\alpha}, \rho_{1,\beta}, \rho_{1,\gamma})$ of the reference antenna are obtained and plotted in Fig. 18. Using the proposed method, the compensated reconstruction of the spherical wave coefficients and radiation pattern of the AUT are obtained and shown in Figs. 19 and 20, respectively. The theoretical gain of the AUT is 9.3 dBi, while the compensated result using the proposed method is 7.2 dBi. The slight gain

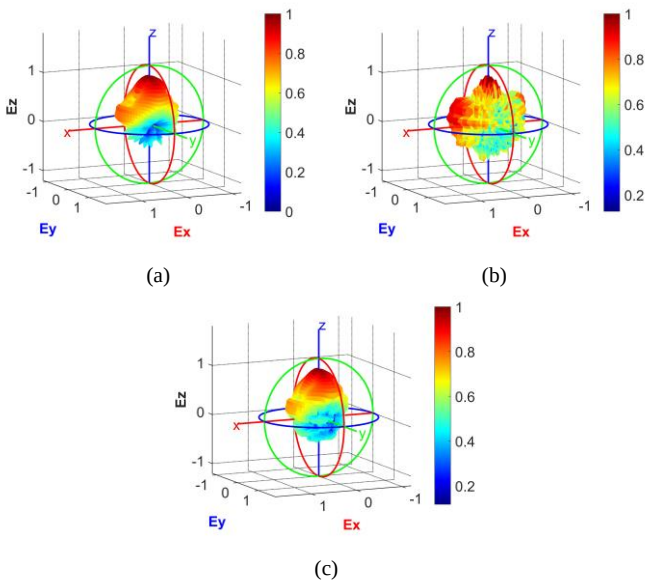

Fig. 20. Radiation pattern of the AUT under the small loaded RC: (a) theoretical pattern; (b) reconstructed pattern using the conventional method; (c) compensated pattern using the proposed method. The maximum value is normalized to 1 V/m for better illustration.

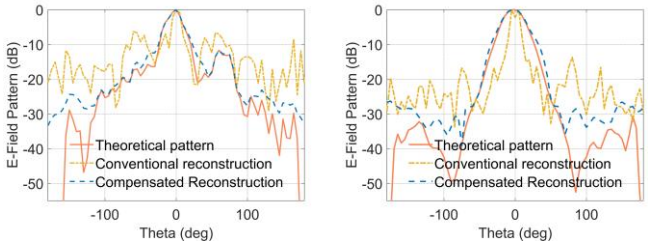

Fig. 21. Comparison of the AUT radiation pattern in (a) E-plane and (b) H-plane.

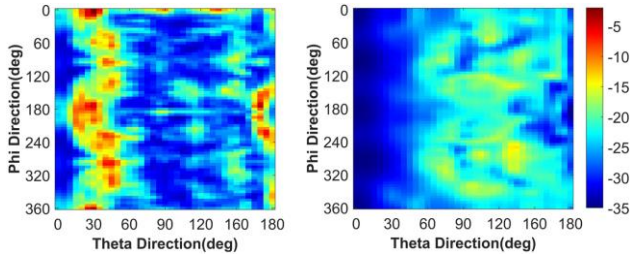

Fig. 22. Comparison of the pattern errors (in dB) between the theoretical AUT pattern and (a) the reconstructed AUT pattern using the conventional method; (b) the reconstructed AUT pattern using the proposed method.

reduction is because that the perturbations (caused by the inevitable antenna stirring due to the small RC size and the increased uncertainty due to the RC loading) tend to increase the sidelobes of the reconstructed pattern. It is apparent that the proposed method improves the reconstructed results. Meanwhile, the cutting plots of the radiation pattern in E- and H- planes are displayed in Fig. 21. From the results of Figs. 20 and 21, it can be seen that the conventional reconstructed pattern of the AUT in the small loaded RC is inconsistent with the theoretical one, while the proposed method has better

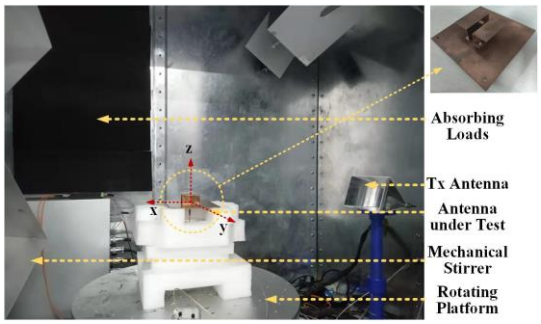

Fig. 23. Correlation coefficients measurement of the magnetoelectric dipole in a small loaded RC.

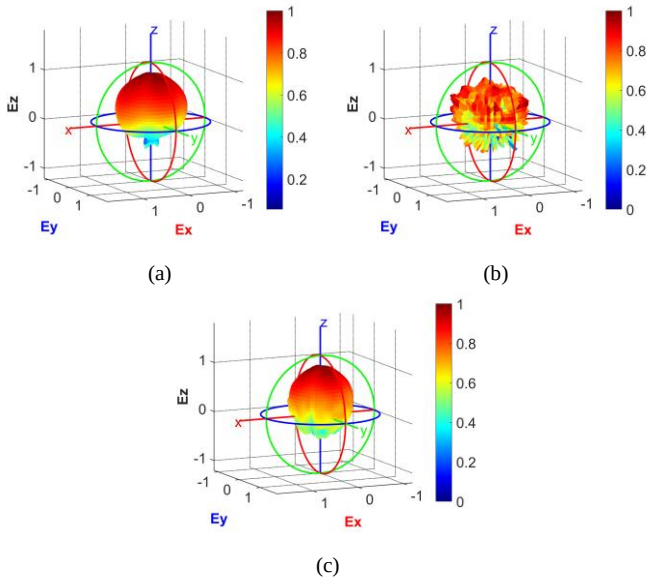

(a) (b)

(c)

Fig. 24. Normalized radiation patterns of AUT 2 in the small loaded RC: (a) theoretical pattern; (b) reconstructed pattern using the conventional method; (c) compensated pattern using the proposed method.

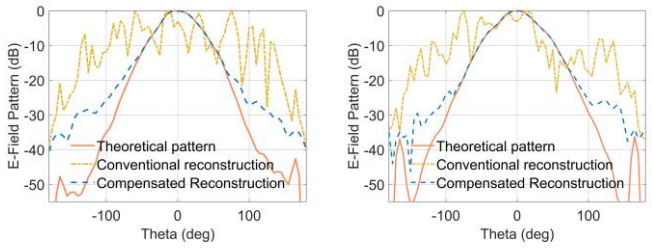

(a) (b)

Fig. 25. Comparison of radiation patterns of AUT 2 in (a) E-plane and (b) H-plane.

accuracy. Besides, the 2-D pattern errors are shown in Fig. 22, indicating that the entire relative spherical errors are decreased when using proposed method in a loaded RC.

2) Small RC and ME Dipole AUT

In order to further verify the effectiveness of the proposed method, an ME dipole antenna is selected as the AUT shown in Fig. 23, and the same reference antenna in the previous experiment is used. The center frequency of the ME-dipole antenna is 2.5 GHz, the number of mechanical stirring N_{Mech} and frequency stirring N_{Freq} are 5 and 200, and the platform

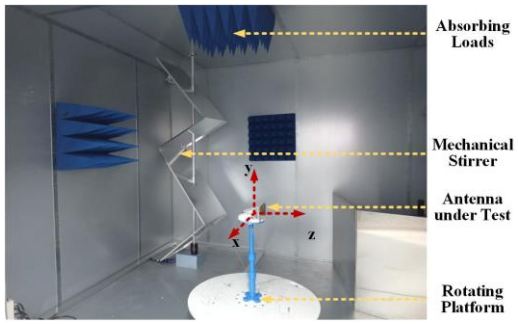

Fig. 26. Photo of a large loaded RC.

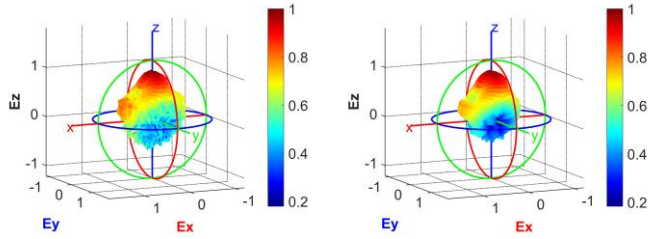

(a) (b)

Fig. 27. Normalized radiation patterns of the AUT 1 in the large unloaded RC: (a) reconstructed pattern using the conventional method; (b) compensated pattern using the proposed method.

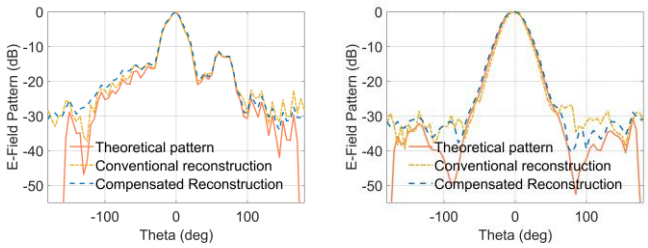

(a) (b)

Fig. 28. Comparison of radiation patterns of AUT 1 in the large unloaded RC in (a) E-plane and (b) H-plane.

rotates 360° with 1° interval.

For convenience, the horn and ME dipole AUTs are denoted as AUT 1 and AUT 2 hereafter, respectively. Thus, by applying the same process shown above, the pattern reconstruction results of AUT 2 (i.e., ME dipole) are shown in Figs. 24 and 25. The measured gain (in the multi-probe anechoic chamber) of AUT 2 is 7.0 dBi, while the compensated gain using the proposed method is 5.6 dBi. According to the results, it can be concluded that the proposed method can compensate for the reconstructed pattern of the AUT in a small loaded RC, and the main lobes shown in Fig. 25 demonstrate the superiority of the proposed method compared with the conventional one in a small loaded RC.

3) Large RC and Horn AUT

In order to better illustrate the impact of the absorbing loads on the results using the conventional method, the uniformity and statistical characteristics of the RC should not be influenced by the rotation of the reference antenna. The influence of the antenna rotation on the field variation can be reduced in a large RC, and the reconstructed results using the

This article has been accepted for publication in a future issue of this journal, but has not been fully edited. Content may change prior to final publication. Citation information: DOI 10.1109/TIM.2022.3151937, IEEE Transactions on Instrumentation and Measurement

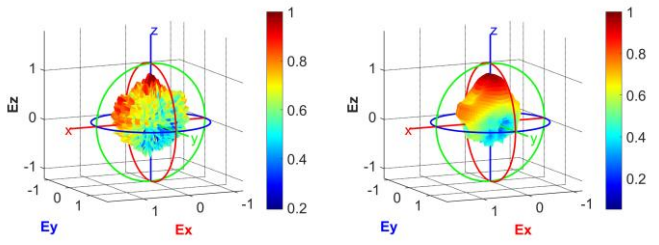

(a) (b)

Fig. 29. Normalized radiation patterns of AUT 1 in the large loaded RC: (a) reconstructed pattern using the conventional method; (b) compensated pattern using the proposed method.

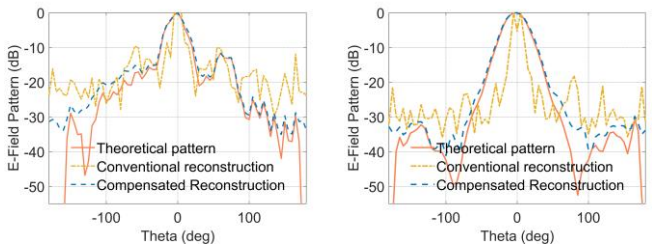

(a) (b)

Fig. 30. Comparison of the radiation patterns of AUT 1 in the large loaded RC in (a) E-plane and (b) H-plane.

conventional method in a large unloaded RC can then be clearly observed. Accordingly, we make the following tests in a well-stirred large RC with a size of 4.2 m × 3.5 m × 2.8 m.

Fig. 26 shows the testing environment of the large loaded RC, while the unloaded environment is realized by removing all the loads of the sidewalls and ceiling. As will be shown later, AUT 2 with wider beamwidth (lower gain) tends to yield a smaller reconstruction error than that of AUT 1. For brevity, only AUT 1 is used to verify the effectiveness of the proposed method in the large RC.

The numbers of mechanical and frequency stirring samples (N_{Mech} and N_{Freq}) are 5 and 200, respectively, and the platform rotates 360° with 1° interval. We perform the same data collection and processing procedures as described above. Then, the reconstructed results using the conventional and proposed methods are obtained and shown in Fig. 27 and Fig. 28. Since the theoretical AUT pattern is the same as Fig. 20(a), only the two reconstructed AUT patterns are displayed in Fig. 27. The antenna gains of the conventional and compensated reconstructed AUT patterns are 8.2 dBi and 8.3 dBi. According to the comparisons of Figs. 27 and 28, it can be seen that, without the influence of the absorbing loads, the adverse effect of antenna rotation on the field uniformity and statistical characteristics can be alleviated, and the reconstructed results of the conventional and proposed methods both have good consistencies with the theoretical one in the large unloaded RC.

The loaded results are shown in Fig. 29 and Fig. 30. The antenna gain obtained using the proposed method is 8 dBi. Through the comparisons of Figs. 27-30, it can be seen that the absorbing loads have a significant impact on the conventional method. Therefore, it can be concluded that the conventional method is not capable of reliably reconstructing the AUT pattern in the presence of absorbing loads.

4) Discussions

In order to further discuss the accuracy of the proposed method, we calculate the relative error between the theoretical and reconstructed patterns using the proposed method

$$D = \frac{\sum_{\theta=-180^\circ}^{180^\circ} \left| E_0(\theta,\varphi) - E_{recon}(\theta,\varphi) \right|^2}{\sum_{\theta=-180^\circ}^{180^\circ} \left| E_0(\theta,\varphi) \right|^2} \tag{15}$$

where $E_0(\theta,\varphi)$ is the theoretical pattern in E- or H-plane (red curves in Figs. 21, 25 and 30), and $E_{recon}(\theta,\varphi)$ is the reconstructed pattern in E- or H-plane using the proposed method in the loaded RC (blue curves in Figs. 21, 25 and 30). Then, the E- and H-plane errors of different AUT and testing environments are shown in Table II

TABLE II
RELATIVE ERRORS BETWEEN THE THEORETICAL AND RECONSTRUCTED PATTERNS USING THE PROPOSED METHOD

	D of AUT 1 in Small Loaded RC (%)	D of AUT 2 in Small Loaded RC (%)	D of AUT 1 in Large Loaded RC (%)
E-Plane	7.29	2.53	6.24
H-Plane	8.41	2.92	2.80

The comparisons of the relative errors show that AUT 2 has a smaller reconstruction error than that of AUT 1 in the small loaded RC. This is because the main lobes dominate the pattern values (where good accuracy can be achieved) and, therefore, AUT 2 with wider beamwidth (lower gain) has a smaller error than that of AUT 1. Hence, the proposed method has better accuracy for less directive antennas. Moreover, the error in the large RC is smaller than that of the small RC, because a large RC volume can reduce the adverse effect of the antenna rotation in the testing environment, as discussed before.

From the measurement results shown above, both the conventional and the proposed methods have errors when compared with the theoretical one. The 3-D pattern errors are calculated and projected into 2-D planes in order to clearly show the deviation of the reconstructed pattern in the conventional and proposed methods. It is clear that the proposed method has a significant improvement of pattern reconstruction as compared with the conventional method. Nevertheless, despite the significant improvement of the proposed method, it can be seen that the agreement between the reconstructed pattern using the proposed method and the measured pattern in the AC is not as good as that in the simulation. The main reason for the discrepancy can be explained as follows: When the size of the RC is small, the rotating antenna on the turntable platform has non-negligible stirring effects as the mechanical mode stirring, which inevitably changes the testing environment of the RC. While the proposed method can effectively mitigate the RC loading effect (as demonstrated in the simulation and measurement sections), the effect of the changing environment cannot be compensated. By using a large RC, this effect can be alleviated to some extent, but there will be still some non-negligible

changes in the testing environment during the antenna rotation. Nevertheless, there are reasonable agreements between the reconstructed pattern using the proposed method and the measured pattern from the AC.

The proposed method can be especially useful for measuring mobile (terminal) antennas, which are typically low-gain antennas with wide beamwidths to ensure good coverage. More importantly, for mobile antenna measurements, the accuracies on small sidelobes are less important [17], [31].

IV. Conclusion

An effective pattern reconstruction method for large well-stirred RCs (i.e., the conventional method) was proposed in the literature. However, the method becomes less effective when the RC is loaded with absorbing materials. Since the RC loading is necessary for OTA tests in general, we proposed an improved pattern reconstruction method for loaded RCs. Specifically, a reference antenna with known radiation characteristics was used to compensate for the RC loading effect. Our simulation results showed that the proposed method can accurately reconstruct the antenna pattern in a loaded RC, as opposed to the conventional method. Our experimental results also demonstrated the superiority of the proposed method to the conventional method. However, the antenna stirring effect became non-negligible in a small RC. This causes a noticeable error in the reconstructed pattern. Nevertheless, this effect can be alleviated by using a large RC, and it is clear that the proposed method has much better accuracy than the conventional method in a loaded RC.

References

[1] J. E. Hansen. *Spherical Near-Field Antenna Measurements*, 1st ed., London: IET, 1988.

[2] M. D. Migliore, F. Soldovieri, and R. Pierri, "Far-field antenna pattern estimation from near-field data using a low-cost amplitude-only measurement setup," *IEEE Trans. Instrum. Meas.*, vol. 49, no. 1, pp. 71-76, Feb. 2005.

[3] V. Rajamani, C. F. Bunting and J. C. West, "Stirred-mode operation of reverberation chambers for EMC testing," *IEEE Trans. Instrum. Meas.*, vol. 61, no. 10, pp. 2759-2764, Oct. 2012.

[4] D. Micheli, M. Barazzetta, F. Moglie, and V. M. Primiani, "Power boosting and compensation during OTA testing of a real 4G LTE base station in reverberation chamber," *IEEE Trans. Electromagn. Compat.*, vol. 57, no. 4, pp. 623–634, Aug. 2015.

[5] X. Chen, W. Xue, H. Shi, et al., "Orbital angular momentum multiplexing in highly reverberant environments," *IEEE Microw. Wireless Compon. Lett.*, vol. 30, no. 1, pp. 112-115, Jan. 2020.

[6] A. Sorrentino, G. Ferrara, and M. Migliaccio, "The reverberating chamber as a line-of-sight wireless channel emulator," *IEEE Trans. Antennas Propag*., vol. 56, no. 6, pp. 1825–1830, Jun. 2008.

[7] M. Á. García-Fernández, J. D. Sánchez-Heredia, A. M. Martínez-González, D. A. Sánchez-Hernández, and J. F. Valenzuela-Valdés, "Advances in mode-stirred reverberation chambers for wireless communication performance evaluation," *IEEE Commun. Mag.*, vol. 49, no. 7, pp. 140–147, Jul. 2011.

[8] P.-S. Kildal, X. Chen, C. Orlenius, *et al.*, "Characterization of reverberation chambers for OTA measurements of wireless devices: physical formulations of channel matrix and new uncertainty formula," *IEEE Trans. Antennas Propag.*, vol. 60, no. 8, pp. 3875 – 3891, 2012.

[9] X. Chen, "On statistics of the measured antenna efficiency in a reverberation chamber," *IEEE Trans. Antennas Propag.*, vol. 61, no. 11, pp. 5417-5424, Nov. 2013.

[10] W. Xue, F. Li, X. Chen, S. Zhu, A. Zhang and T. Svensson, "A unified approach for uncertainty analyses for total radiated power and total isotropic sensitivity measurements in reverberation chamber," *IEEE Trans. Instrum. Meas.*, vol. 70, pp. 1-12, 2021.

[11] V. Fiumara, A. Fusco, V. Matta and I. M. Pinto, "Free-space antenna field/pattern retrieval in reverberation environments," *IEEE Antennas Wireless Propag. Lett.*, vol. 4, pp. 329-332, 2005.

[12] P. Besnier, C. Lemoine, J. Sol and J. Floc'h, "Radiation pattern measurements in reverberation chamber based on estimation of coherent and diffuse electromagnetic fields," in *Proc. IEEE Conf. Antenna Meas. Appl. (CAMA)*, 2014, pp. 1-4.

[13] C. Lemoine, E. Amador, P. Besnier, J. Floc'h and A. Laisné, "Antenna directivity measurement in reverberation chamber from Rician K-factor estimation," *IEEE Trans. Antennas Propag.*, vol. 61, no. 10, pp. 5307-5310, Oct. 2013.

[14] M. Á. García-Fernández, D. Carsenat and C. Decroze, "Antenna radiation pattern measurements in reverberation chamber using plane wave decomposition," *IEEE Trans. Antennas Propag.*, vol. 61, no. 10, pp. 5000-5007, Oct. 2013.

[15] M. Á. García-Fernández, D. Carsenat and C. Decroze, "Antenna gain and radiation pattern measurements in reverberation chamber using doppler effect," *IEEE Trans. Antennas Propag.*, vol. 62, no. 10, pp. 5389-5394, Oct. 2014.

[16] Q. Xu, Y. Huang, et al., "3-D antenna radiation pattern reconstruction in a reverberation chamber using spherical wave decomposition," *IEEE Trans. Antennas Propag.*, vol. 65, no. 4, pp. 1728-1739, Apr. 2017.

[17] P. Shen, Y. Qi, W. Yu, J. Fan and F. Li, "OTA measurement for IoT wireless device performance evaluation: challenges and solutions," *IEEE Internet Things J.*, vol. 6, no. 1, pp. 1223-1237, Feb. 2019.

[18] M. G. Becker, R. D. Horansky, D. Senic, V. Neylon and K. A. Remley, "Spatial channels for wireless over-the-air measurements in reverberation chambers," in *Proc. 12th Eur. Conf. Antennas Propag.*, 2018, pp. 1-5.

[19] P. Hallbjorner, "Accuracy in reverberation chamber antenna correlation measurements," *Int. Workshop Antenna Technol., Small Smart Antennas Metamater. Appl. (IWAT)*, 2007, pp. 170-173.

[20] X. Chen, P. S. Kildal and J. Carlsson, "Comparisons of different methods to determine correlation applied to multi-port UWB eleven antenna", in *Proc. 5th Eur. Conf. Antennas Propag.*, Apr. 2011, pp. 1776-1780.

[21] T. B. Hansen, "Correlation and capacity calculations with reference antennas in an isotropic environment," *Int. J. Antennas Propag.*, vol. 2012, pp. 184-195, May 2012.

[22] H. L. Thal and J. B. Manges, "Theory and practice for a spherical-scan near-field antenna range," *IEEE Trans. Antennas Propag.*, vol. 36, no. 6, pp. 815-821, June 1988.

[23] J. L.-W. Li, W.-L. Ong and K. H. R. Zheng, "Anisotropic scattering effects of a gyrotropic sphere characterized using the T-matrix method," *Phys. Rev. E*, vol. 85, no. 3, p. 036601, Mar. 2012.

[24] Y. Song, C. Tse and C. Qiu, "Electromagnetic scattering by a gyrotropic-coated conducting sphere illuminated from arbitrary spatial angles," *IEEE Trans. Antennas Propag.*, vol. 61, no. 6, pp. 3381-3386, June 2013.

[25] Y.-L. Geng, "Scattering of a plane wave by an anisotropic ferrite-coated conducting sphere," *IET Microw. Antennas Propag.*, vol. 2, pp. 158-162, 2008.

[26] C. Qiu, S. Zouhdi and A. Razek, "Modified spherical wave functions with anisotropy ratio: application to the analysis of scattering by multilayered anisotropic shells," *IEEE Trans. Antennas Propag.*, vol. 55, no. 12, pp. 3515-3523, Dec. 2007.

[27] Z. Romanowski and S. Krukowski, "Transformation of complex spherical harmonics under rotations," *J. Phys. A: Math. Theor.*, vol. 40, no. 50, p. 15071, Nov. 2007.

[28] D. N. Black and E. B. Joy, "Test zone field compensation," *IEEE Trans. Antennas Propag.*, vol. 43, no. 4, pp. 362-368, Apr. 1995.

[29] J. T. Toivanen, T. A. Laitinen and P. Vainikainen, "Modified test zone field compensation for small-antenna measurements," *IEEE Trans. Antennas Propag.*, vol. 58, no. 11, pp. 3471-3479, Nov. 2010.

[30] K. Luk and B. Wu, "The magnetoelectric dipole—a wideband antenna for base stations in mobile communications," *Proc. IEEE*, vol. 100, no. 7, pp. 2297-2307, July 2012.

[31] Z. Chen. *Antennas for Portable Devices*, Wiley Press, 2007.